nature chemical biology

ARTICLE

PUBLISHED ONLINE: 14 OCTOBER 2014 | DOI: 10.1038/NCHEMBIO.1680

Digital switching in a biosensor circuit via programmable timing of gene availability

Nicolas Lapique & Yaakov Benenson*

Transient delivery of gene circuits is required in many potential applications of synthetic biology, yet the pre-steady-state processes that dominate this delivery route pose major challenges for robust circuit deployment. Here we show that site-specific recombinases can rectify undesired effects by programmable timing of gene availability in multigene circuits. We exemplify the concept with a proportional sensor for endogenous microRNA (miRNA) and show a marked reduction in its ground state leakage due to desynchronization of the circuit's repressor components and their repression target. The new sensors display a dynamic range of up to 1,000-fold compared to 20-fold in the standard configuration. We applied the approach to classify cell types on the basis of miRNA expression profile and measured >200-fold output differential between positively and negatively identified cells. We also showed major improvements in specificity with cytotoxic output. Our study opens new venues in gene circuit design via judicious temporal control of circuits' genetic makeup.

Many cellular pathways are controlled by external molecular inputs via natural biosensor molecules, such as cell surface receptors and transcription factors[1]. Engineered biosensing circuits are likewise increasingly used in basic research[2,3], bioproduction[4] and medicine[5,6]. Research in synthetic biology has greatly expanded the repertoire of tools for biosensor engineering with the development of toggle switches[7,8], band-pass filters[9], open-loop sensors[10], riboswitches[11], time-delay circuits[12] and oscillators[13,14]. Perhaps the most basic mode of sensing is proportional sensing[15], where increasing levels of input signal elicit higher levels of sensor output. For inputs with natural repressor function, such as small-molecule inhibitors, miRNA or transcriptional repressors, proportional sensing can be implemented with a synthetic 'double inversion' module capable of suppressing the output expression while being suppressed by the input[16–19] (**Fig. 1a**). A simple way to characterize a sensor is to measure its 'off' and 'on' states in the absence and presence of an input, respectively. Achieving large dynamic range, that is, the on/off ratio, with an appropriately designed double-inversion sensor has been shown with exogenous ligand IPTG[17], but the range is more modest with the reported sensors for endogenous miRNA inputs[18].

Some of these sensors can be potentially applied to diagnostics and gene therapy[20]. These scenarios require transient delivery of sensor-encoding genes using physico-chemical methods or viral vectors[21]. During transient delivery, system behavior is dominated by pre-steady-state processes that take place as the delivered genes become expressed and their products start interacting with each other and with cellular components. A particular challenge in sensors based on a double-inversion module is the simultaneous expression of the repressor components and their target output gene. Because the output does not initially 'experience' the repressor action owing to the absence of repressor, its concentration overshoots early in the process (i.e., a pulse is generated) even when the repressor is potent[22–24]. In addition, transient delivery causes variability in gene copy number between cells, resulting in large cell-to-cell variability of the 'on output', which is typically proportional to the copy number of the output-encoding gene unless special compensation mechanisms are put in place[25]. Thus, the off state is the prime target for sensor optimization and the improvement of the dynamic range.

Output pulse is a weakness of the double-inversion strategy because even transient output expression can have physiological effects, and a stable protein output may linger in the cell for a long time. As the pulse results from simultaneous commencement of gene expression, it could be possible to address the problem by desynchronizing the production of the repressor and the output species and creating a 'buffer'[26] of repressor early on. This can be achieved by temporal control of the circuit's genes, for example, by providing the repressor genes before the output genes. However, the application-imposed constraint regarding autonomous delivery of all system components requires that whatever tool is used to control the timing must itself be delivered together with the rest of the system. Here we demonstrate how temporal control of the circuit components can be implemented with site-specific recombinase delivered together with the sensor genes, leading to a marked improvement in sensor operational parameters. In particular, we delayed the availability of the output components, leading to early accumulation of repressor molecules and almost undetectable leakage in the off state with fluorescent output. We performed a thorough mechanistic investigation of this strategy and showed excellent digital performance in the cell classification task. Furthermore, we demonstrated that this approach greatly improved the selectivity of the very sensitive downstream physiological actuator, thymidine kinase from herpes simplex virus (HSV-TK), in combination with the prodrug ganciclovir.

RESULTS

The cause of leakage in the sensor

Our previously reported double inversion module (**Fig. 1b**) features (i) a gene that encodes a constitutively expressed rtTA activator and (ii) an rtTA-controlled gene coding for a LacI repressor and an intronic, engineered miRNA known as miR-FF4 (ref. 18). LacI and miR-FF4 repress the output gene transcriptionally and post-transcriptionally, respectively. Both rtTA and LacI transcripts contain tandem repeats of perfectly complementary targets of a miRNA input of interest. Thus, in the absence of a miRNA input, highly expressed rtTA induces both LacI and miR-FF4, which in

Department of Biosystems Science and Engineering, Swiss Federal Institute of Technology Zurich (ETHZ), Basel, Switzerland.
*e-mail: kobi.benenson@bsse.ethz.ch

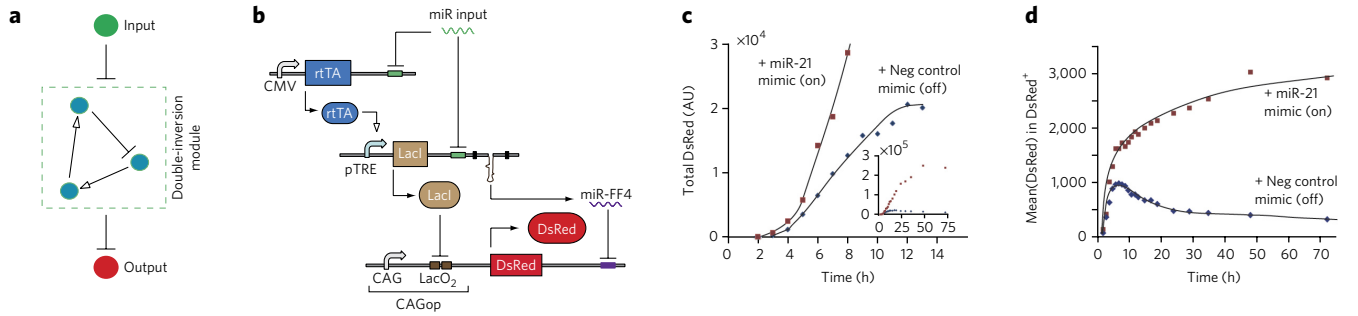

Figure 1 | Source of leakage in the proportional sensor. (**a**) General layout of a proportional sensor for a negative regulator. An input elicits inhibitory effect on a double-inversion module, which in turn negatively regulates the output. (**b**) Circuit diagram of the proportional miRNA sensor, as previously reported[18]. Pointed arrows indicate activation, and blunted arrows denote repression. Rectangles targeted by miRNA represent four identical sites for miR-21 and three identical sites for miR-FF4. pTRE, TRE promoter. (**c**) Total output signal shown as a function of time in both on (+ miR-21 mimics) and off (+ negative (neg) control mimics) sensor states. The signal is the sum of all DsRed intensities in DsRed-positive cells. The signal was not normalized because the expression of the transfection marker AmCyan showed very similar dynamics in all cases. Inset, time course over 72 h. AU, absolute units. (**d**) Mean fluorescence of DsRed-expressing cells in off (blue) and on (red) states, respectively, as a function of time. The curves were drawn manually to serve as guides.

turn repress the output. When the miRNA input of interest is highly expressed, rtTA is strongly knocked down, and thus LacI and miR-FF4 are not expressed. In addition, LacI is knocked down separately by the same miRNA input. This sequence of events enables output expression from the LacI-controlled promoter.

Previously, we observed sensor leakiness in the off state, even when the overall dynamic range (on/off) was high. Leakiness in the off state, regardless of the dynamic range, is undesirable because downstream processes could be highly sensitive to low, transient amounts of output. We established a new assay system to study the causes for sensor leakiness and optimize its performance. The assay comprises HEK293 cells that naturally express only trace amounts of miR-21 (ref. 18). We used the miR-21 sensor with DsRed fluorescent output, generating the sensor 'on state' by cotransfecting saturating levels (10 pmol) of miR-21 mimic into the cells (**Supplementary Results**, **Supplementary Fig. 1a**). To evaluate the off state, we used a similar molar amount of the negative control miRNA mimic.

Using this assay, we performed time-course measurements of the sensor response in both on and off states using transient transfection. Sensor dynamics revealed that in both states, the early-expressing cells displayed very similar kinetics in the first few hours (0–5 h) before progressively diverging (**Fig. 1c,d** and **Supplementary Fig. 1b**), with the 'off output' (mean output intensity in output-positive cells) displaying the characteristic pulse kinetics (**Fig. 1d**). This observation was qualitatively consistent with earlier findings regarding the delay between the expression of a repressor protein[27] or a miRNA[28] and the response of their target. The off output pulse peaked around 5–6 h (**Fig. 1d**); thus, we hypothesized that a delay of 6–10 h in the output gene availability and the commencement of output gene expression might substantially reduce the leakage.

Introducing a delay in output availability

A number of approaches could be envisioned to delay output production[12,29]. Although control over gene expression timing using transcriptional regulation is one option, the most drastic and 'clean' intervention would be to withhold the gene itself. This requires programmable, time-dependent modification in the circuit-encoding DNA, which is best achieved through DNA-manipulating enzymes such as recombinases. Therefore, we opted for a recombinase-driven inversion of the output-coding region relative to its promoter. A Cre-Lox recombination system was engineered to delay output production using the FLEx switch, which exploits the dual inversion and excision activity of the recombinase[30]. Using two pairs of incompatible Lox recombination sites, the coding region of the output sequence is stably and irreversibly inverted after Cre-mediated recombination (**Fig. 2a**). In the 'delayed' sensor, the standard output construct was replaced with a backward-facing DsRed coding region; a constitutive Cre expression cassette was included with other circuit components. The delay amounted to 6–8 h (**Fig. 2b**). As a result, we observed a marked effect on the sensor off state (**Fig. 2c–e**), in which virtually all fluorescent leakage was eliminated, whereas the on state was only moderately reduced. This reduction in the on state could largely be explained by incomplete inversion of the backward-facing output (**Supplementary Fig. 2a,b**). There was an overall improvement of about 30-fold in the dynamic range of the sensor (**Fig. 2c**). We note parenthetically that cotransfection of the negative control mimic, which is the appropriate off state measurement while using the miR-21 mimic, increased the off state of the standard sensor and, to a lesser extent, in the delayed sensor. Yet even when the negative control mimic was withheld (**Fig. 2c**), the off state was improved by approximately an order of magnitude.

Control of the timing

We observed that a greater amount of recombinase-encoding plasmid accelerated recombination (**Supplementary Fig. 2c**) and proceeded to investigate the effect of this plasmid dosage on the leakage and the dynamic range of the sensor. The 'on signal' (**Fig. 3a**) fits the Hill function with $n = 1$ and an apparent half-maximum effective concentration on the order of 2 ng, regardless of the quantification method (**Supplementary Fig. 3**). The off output depended on the amount of recombinase in an almost linear fashion (off ~$[Cre]^{0.77}$; **Fig. 3a**), resulting in an on/off ratio at lower recombinase levels of >2,000 (**Fig. 3a**). In the experiments described henceforth, we used 5 ng of the plasmid encoding the EF1α-driven iCre gene after optimization, unless indicated otherwise. At low plasmid levels of recombinase-encoding construct, the reduction in the on output could be explained by reduced cotransfection efficiency of the recombinase and its target. To modulate Cre expression without affecting cotransfection efficiency, we used an inducible promoter driven by an ET1 transactivator whose activity can be controlled by the antibiotic erythromycin[31] (**Supplementary Fig. 4**). Similarly to plasmid titration, modulation of Cre activity showed that the off level increased with increased recombinase expression, but the on output was constant in the promoter activity range (**Fig. 3b**).

We also tested whether the leakage in the off state could be further reduced with additional chemical-induced delay. We used a Cre recombinase with estrogen receptors (ERs)[32] fused at its C and N termini. Cre translocation into the nucleus is enabled upon addition of tamoxifen, and hence recombination can only occur in the presence of this drug. We used a large amount of the fusion protein and delayed its activity by withholding tamoxifen. This experiment showed that the off output was reduced upon extended delay, leading to a larger

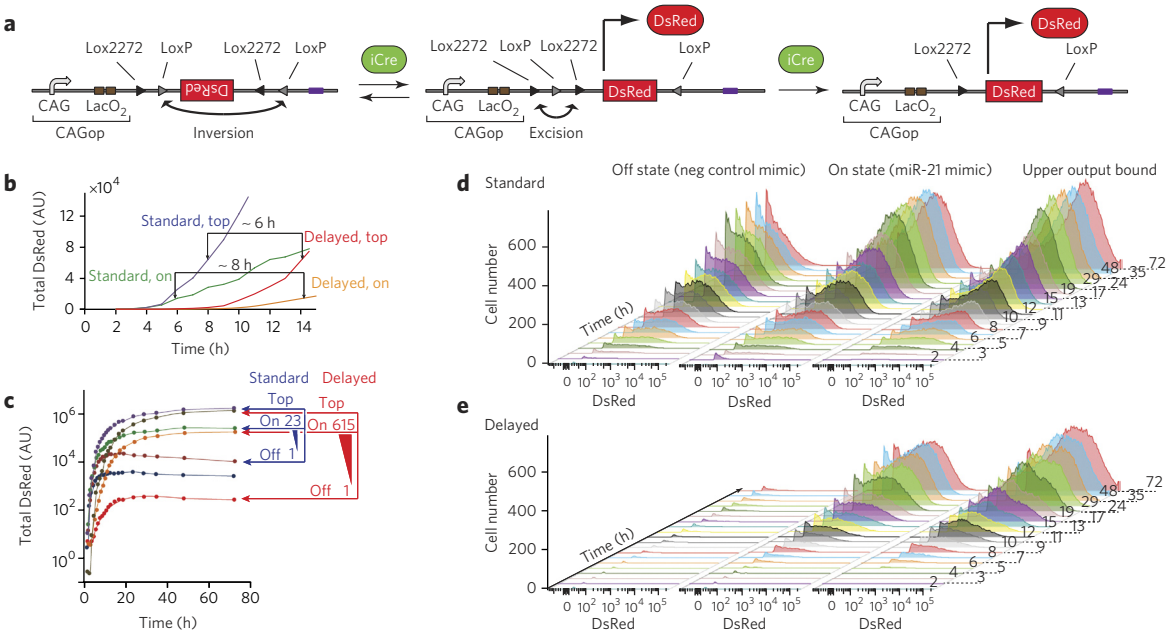

Figure 2 | The effect of delayed output on sensor performance. (**a**) The principle behind the FLEx inversion system[30]. (**b**–**e**) Time course measurements of standard and delayed sensor architectures. (**b**) Time course of total output protein expression from the uncontrolled forward-facing output gene (standard, top, blue line) and delayed output expression from uncontrolled backward-facing output gene (delayed, top, red line), showing an ~6-h delay. Comparison of the on signal development in the standard (standard, on, green line) and the delayed (delayed, on, orange line) sensor displayed an 8-h delay. Only the first 14 h are shown. AU, absolute units. (**c**) Time course of total DsRed signal corresponding to the uncontrolled output gene (top), miR-21 sensor in the presence of miR-21 mimic (on state) and sensor in the presence of negative (neg) control mimic (off state), corresponding to both standard and delayed configurations, as indicated in the chart, over 72 h. The fold ratios between the on and the off signals are shown. The blue curve corresponds to the off state of the standard sensor in the absence of any miRNA mimic. (**d**) Time-dependent histograms of DsRed output in the standard sensor configuration. Different setups are indicated on top. The label 'upper output bound' corresponds to DsRed expression from uncontrolled output gene (same as 'top' in **b** and **c**). (**e**) Time course measurements in the delayed configuration. The time series are as in **d**.

dynamic range. The on signal is largely constant and only decreases slightly when the drug is added 24 h after transfection, probably owing to the shorter time available for recombination (**Fig. 3c**).

An approach to extend the delay autonomously without reverting to chemical ligands is to build a recombination cascade. We used a second site-specific recombinase Flp and Flp-compatible FLEx cassette to flank the Cre gene (**Fig. 3d**). To increase cotransfection of both recombinases, we used a large amount of Cre-expressing plasmid (25 ng) in the standard, delayed (Cre) and Flp-Cre strategies. In a side-by-side comparison, the use of two recombinases resulted in a dynamic range of ~1,500 and a tenfold improvement relative to the use of one recombinase with a similar amount of plasmid. Fine tuning is likely to improve the range.

Alternatives to recombinase-induced delay

The results in **Figure 3** unequivocally indicate that the improvement in the off state is the direct consequence of the delay in output gene availability and that the dynamic range of the sensor could be controlled by a variety of methods, including Cre gene dosage, control of Cre gene expression, control of Cre protein translocation or a recombination cascade. We examined the possibility of establishing a similar delay without the recombinase by using sequential physical delivery of circuit genetic components, specifically by sequential transfection of the miR-21–targeted rtTA and LacI–miR-FF4 genes followed by the output gene. Because the DNA transfected at each step is loaded in separate liposomes, DsRed output and AmCyan control (transfected together with the rtTA and LacI–miR-FF4 genes) had a very low correlation compared to that resulting from simultaneous transfection (**Supplementary Fig. 5**). This also explained the poor output repression resulting from the sequential transfection, whose overall performance was greatly inferior to that of the Cre-induced delay, emphasizing the importance of simultaneous and correlated delivery of genetic components. An alternative approach to dynamic range improvement could be accelerated delivery of the repressor by adding a short interfering RNA (siRNA) equivalent of miR-FF4 to generate strong knockdown at time zero. Indeed, even small amounts of siRNA-FF4 (0.5 pmol) strongly reduced leakage of standard sensor with a moderate reduction of the on state, leading to a better dynamic range (**Supplementary Fig. 6**). However, although a further increase in siRNA amount reduced the leakage, it also reduced the on state by a similar fraction without a large improvement in the on/off ratio. The on state in the standard sensor is achieved by knockdown of rtTA with a miRNA input, such that the repressors LacI and miR-FF4 are never present at high levels. With siRNA-FF4, a large amount of repressor is introduced in both off and on input states, and full dilution or degradation of this siRNA would be required for high on state.

To conclusively eliminate any alternative explanation for leakage suppression in the off state, we performed two more control experiments. First, we evaluated whether the antisense DsRed transcripts generated from backward-facing output genes sequestered forward-facing output transcripts. However, we did not observe a discernible effect when compared to the inert 'stuffer' DNA (**Supplementary Fig. 7**). Second, we checked whether the effect could be attributed simply to the reduction of the output gene dosage relative to double-inversion module genes owing to incomplete recombination. We measured sensor performance with different ratios of inverted and forward-facing output genes in the absence of Cre recombinase. Data in **Supplementary Figure 8a–d** showed that though the off state improved when the forward-facing output was reduced, the on output was reduced comparably, leaving the on/off ratio largely constant. Thus, using the recombinase reduces the leakage in the

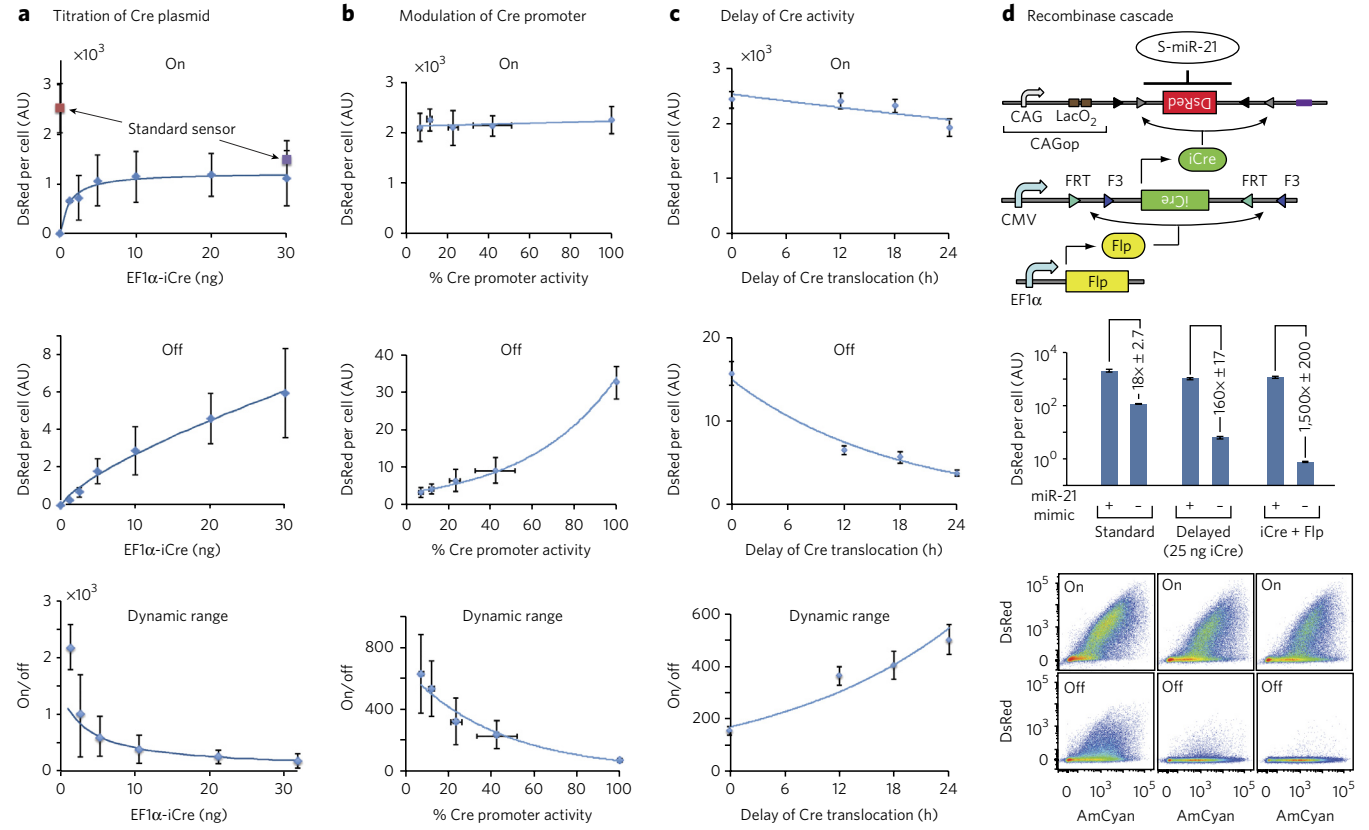

Figure 3 | Control of the timing. (**a**–**c**) The rows in the top, middle and bottom charts correspond to the on state, off state and on/off ratio, respectively. The on/off curves are calculated by dividing the fitted curve of the on measurement by the fitted curve of the off measurement. (**a**) Delayed sensor characterization as a function of Cre-expressing plasmid amount. The curves are fitted to the Hill function with $n = 1$ (on states) and to the power law (off states). AU, absolute units. (**b**) Modulation of Cre expression with an inducible promoter. ETR-iCre activity was ascertained from the ETR-DsRed reporter with various concentrations of erythromycin (**Supplementary Fig. 4**). The *x* axis shows the percentage of promoter activity relative to full activity in the absence of erythromycin. The curves are fitted to linear (on states) and exponential (off states) regressions. (**c**) Chemical delay of ER2-Cre-ER2 translocation. The *x* axis shows the time between the transfection and the addition of tamoxifen. The curves are fitted to linear (on states) and exponential (off states) regressions. (**d**) The recombinase cascade eliminates the leakage. The sensor diagram is shown at top. The bar chart compares standard architecture with a Cre-only delayed architecture to a cascade system, with the representative flow cytometry scatter plots shown on the bottom. Error bars show ± s.d. from at least three biological replicas.

off state without the concomitant decrease in the on state that is observed with alternative approaches (**Supplementary Fig. 8e**,**f**).

Functional dissection of sensor components

The cumulative evidence shown above strongly favors the hypothesis that the recombinase-induced delay enables the double-inversion module to produce enough repressor molecules before the commencement of output expression, thus greatly reducing the leakage. Next we asked which molecular features of the double-inversion module contributed most to this phenomenon. The repressor exerts transcriptional and post-transcriptional control using LacI protein and an artificial spliced miRNA (miR-FF4), respectively. We already showed that siRNA-FF4 had a very strong inhibitory effect of its own (**Supplementary Fig. 6**). We mutated either the LacI or the miR-FF4 component (**Fig. 4a**,**b**), confirmed their loss of function (**Supplementary Fig. 9**) and measured sensor performance in both standard and delayed configurations (**Fig. 4c**). The data showed that though the LacI–miR-FF4 combination was the best performer, the LacI mutant still generated most of the total repression capacity via miR-FF4. In the delayed configuration, it exhibited a dynamic range of more than two orders of magnitude, and likewise in the standard setting the effect of LacI removal was relatively minor. In contrast, removing miR-FF4 had a major detrimental effect on both delayed and standard architectures. This indicates that an efficient repressor is a necessary prerequisite for high dynamic range in both standard and delayed configurations.

To further improve our understanding of the sensor mechanism, we removed the activator rtTA and replaced the TRE promoter of the LacI–miR-FF4 construct with a constitutive cytomegalovirus (CMV) promoter (**Supplementary Fig. 10**). We conjectured that removing rtTA induction would accelerate the expression of LacI and miR-FF4, thus improving the off state to the level observed otherwise with Cre-induced delay. However, we only found a twofold reduction of the leakage relative to both the complete and $LacI^{mut}$ standard sensors. The leakage was further reduced when CMV was replaced by a stronger CAG promoter driving LacI–miR-FF4 (**Supplementary Fig. 10**). Yet, in line with expectations, without the upstream transcriptional activator the repressor module of the sensor remained active despite the knockdown by miR-21, and the on state stayed very low because the miR-FF4 level was not affected by RNAi knockdown of LacI that occurred after the splicing of miR-FF4 (ref. 33). For the same reason, we expected that the on and the off states would be identical in the LacI mutant. Interestingly, we observed weak but reproducible derepression even when LacI was mutated. One explanation is that in dividing cells such as HEK293, the strict separation between nucleus and cytoplasm is not maintained all the time, and thus even unspliced LacI-miR-FF4 transcript could be targeted by miR-21. To summarize, compared to standard sensors, repression can be slightly

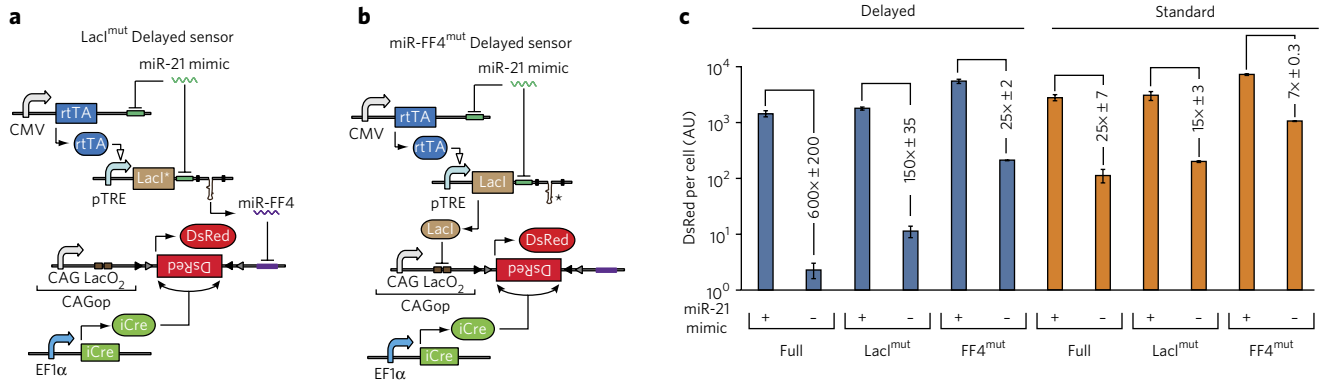

Figure 4 | Component contribution to sensor performance. (**a**–**c**) Circuit diagrams of the LacI mutant sensor (**a**), miR-FF4 mutant sensor (**b**) and their relative performance (**c**). Asterisks indicate mutated components. AU, absolute units. Error bars show ± s.d. from at least three biological replicas.

improved without the upstream transcriptional activator, but the latter is essential for the sensor derepression to a high on state. This is consistent with the finding that most of the repressing effect comes from miR-FF4, and the only way to reduce miR-FF4 levels using another miRNA is by targeting its transcriptional activator.

We next asked whether individual circuit building blocks could be exchanged. First, we replaced the LacI-controlled CAGop promoter with the CMV promoter, and second, we replaced the DsRed output gene with ZsYellow (**Supplementary Fig. 11**). In both of these modifications, the delayed circuit showed a large improvement in the off state relative to the standard configuration, as expected. Replacing DsRed with ZsYellow did not affect the performance, suggesting that the sensor can be used to control different output genes. The sensor with the CMV promoter showed poor performance, in large part because of lower knockdown efficiency by miR-FF4, consistent with our earlier observations[34].

Using delayed sensors for cell classification

Cell classification[18], or precise cell targeting based on complex signatures of endogenous markers such as miRNAs, has emerged as a promising development in mammalian synthetic biology with possible applications ranging from cell reprogramming to selective therapeutic agents. Any circuit architecture intended for this task must operate robustly in different mammalian cell types. To validate our approach in this scenario, we assembled a simplified version of the published HeLa classifier[18] using two HeLa-high sensors for miR-21 and a composite marker, miR-17-30a, computing the logic AND gate '(miR-21) AND (miR-17-30a)'. We first tested the miR-21 sensor alone, together with on and off constitutive controls (**Fig. 5a**). In HeLa cells with EF1α-driven Cre (**Fig. 5b**), the basic recombination efficiency of the inverted output was poor (~35% relative to forward-facing 'constitutive on' control; **Fig. 5c**). Therefore, the expression level of the delayed miR-21 sensor in HeLa cells was also impaired (**Fig. 5c** and **Supplementary Fig. 12**), even though we still observed an improved output ratio between HEK293 and HeLa cells. The reason for this could be poor cotransfection in HeLa cells, given the low molar ratio of EF1α-iCre cassette to output. To increase the amount of Cre plasmid without increasing recombinase levels, we exchanged the strong EF1α promoter with a weaker promoter, SV40 (**Fig. 5b**). The SV40-iCre cassette was used in 1:2 molar ratio to the output plasmid, enabling a much better signal recovery in HeLa cells (**Fig. 5c** and **Supplementary Fig. 12**). In addition, with this new setup, the leakage in HEK293 cells was even lower than with the EF1α-iCre cassette, resulting in an ~400-fold differential expression between HEK293 and HeLa cells. To eliminate the consequences of imperfect Cre plasmid cotransfection, we embedded the SV40-iCre expression cassette and the output gene on the same plasmid (**Fig. 5b**). A mammalian promoter could have basal activity in prokaryotic cells[35], and thus to avoid recombination during plasmid amplification in *Escherichia coli*, we placed an intron in the coding sequence of the recombinase. Interestingly, this configuration improved sensor performance even without delay (**Fig. 5c** and **Supplementary Fig. 12**), via slight reduction of leakage in HEK293 and improvement in the on state in HeLa cells. The delayed miR-21 sensor using a single backbone gave the highest HeLa/HEK293 output ratio, with a fold difference of ~500; therefore, this configuration was tested in the extended AND gate classifier circuit configuration. In this latter case (**Fig. 5d** and **Supplementary Fig. 13**), we observed an excellent output ratio of about 250-fold between the cell lines with the delayed sensor. Owing to the same backbone configuration, the loss of circuit output in HeLa cells due to incomplete recombination was only about 10%.

Control of highly potent physiological output

Lastly, we tested the ability of the delayed sensor to selectively cause cell death in the presence of high miR-21, with the fluorescent output gene replaced by the gene encoding HSV-TK. This enzyme can induce cytotoxicity when acting on the prodrug ganciclovir, and the phosphorylated prodrug can be toxic to the cell expressing the enzyme as well as to bystander cells[36]. The combination of enzymatic actuation with the bystander effect is a very sensitive reporter of leakage, and we measured cytotoxicity using the total number of surviving cells. Cell viability was measured with the live-cell staining reagent Calcein AM, and the number of live cells was measured by flow cytometry (Online Methods). First, we tested the miR-21 sensor in the standard and delayed configurations with miR-21 mimics in HEK293 cells (**Fig. 6a** and **Supplementary Fig. 14**). We used the exact same configuration (plasmid amounts, cell numbers and growth conditions) as for the fluorescent output, except the time between the transfection and the measurement was extended from 3 d to 5 d to allow the manifestation of cytotoxic effect. Using the standard miR-21 sensor configuration, the cytotoxicity on the whole-population level was strong, and on (miR-21^{POS}) and off (miR-21^{NEG}) states were very similar (**Fig. 6a** and **Supplementary Fig. 14**). The cytotoxicity observed with constitutive expression of inverted HSV-TK plus Cre was less marked than with forward-facing TK, but it still had a killing efficiency of 92%. With the delayed miR-21 sensor, we could observe an expected trend, with most cells surviving in the off state compared to the on state (**Fig. 6a** and **Supplementary Fig. 14**). Though the numbers are not perfect and the variability is high, there was marked improvement over the standard configuration.

Next, we attempted to translate differential expression of fluorescent output to selective cytotoxicity in different cell lines. We first tried to use the HEK293-HeLa combination, but HSV-TK failed to show a toxic effect on HeLa cells, presumably owing to a poor bystander effect in this cell line[37]. Thus we looked into a few other

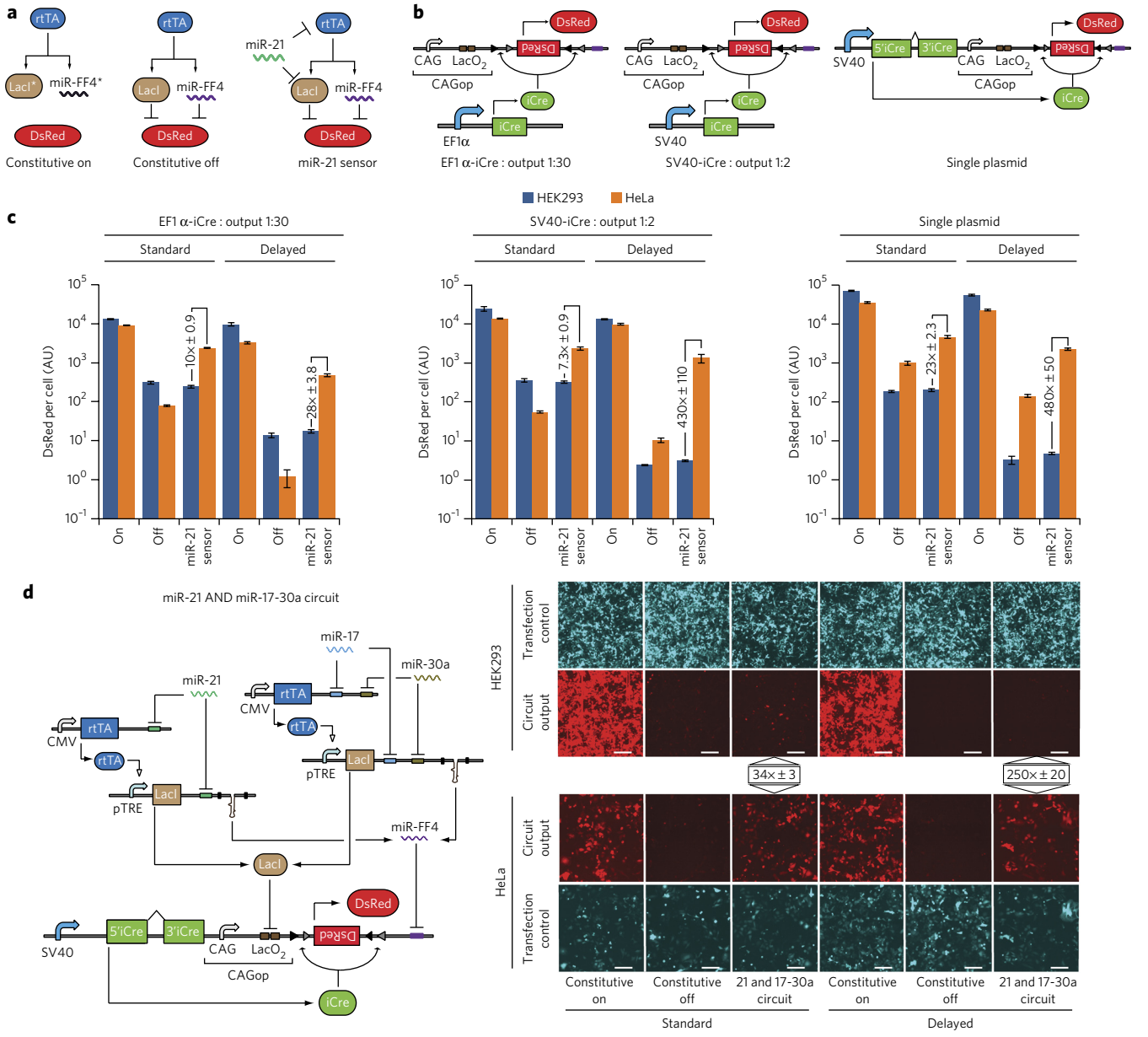

Figure 5 | Cell type classification. (**a**,**b**) Schematics of tested sensors and controls (**a**) and delayed output variants (**b**). (**c**) Output in HeLa cells relative to HEK293 cells. Each bar chart compares output intensity in HEK293 and HeLa cells using a particular output variant with three sensor variants (constitutive on (on), constitutive off (off) and miR-21 sensor) in forward-facing and delayed configurations. Flow cytometry plots are shown in **Supplementary Figure 12**. AU, absolute units. (**d**) A version of a HeLa cell classifier encoding the '(miR-21) AND (miR-17-30a)' logic gate. Delayed and standard circuits have the SV40-iCre cassette embedded on output plasmid. Representative microscopy snapshots show transfection control (cyan) and circuit output (red). Each panel compares HEK293 with HeLa with three different circuit variants (on, off and actual logic circuit) in standard and delayed configurations. Flow cytometry scatter plots are in **Supplementary Figure 13**. Error bars show ± s.d. using at least three biological replicas. Scale bars, 200 μm.

cancer cell lines, namely HCT-116 and HuH-7, both expressing high levels of miR-21. We first tested the fluorescent sensor using the SV40-iCre split plasmid configuration. Both cell lines showed high output compared to HEK293 cells (**Supplementary Fig. 15**). Preliminary tests showed 50% killing of HuH-7 cells and 80% killing of HCT-116 cells by constitutive HSV-TK (data not shown), consistent with cytotoxicity reported in the literature[38,39]; thus, we chose HCT-116 cells for comparison with HEK293 cells (**Fig. 6b** and **Supplementary Fig. 16**). With the standard sensor, different configurations generated similar levels of toxicity. The delayed miR-21 sensor in HCT-116 cells had toxicity similar to that of the constitutive HSV-TK expressed without delay, meaning that the sensor used most of its potential. Interestingly, the delayed constitutive off sensor in HEK293 cells leads to almost complete cell survival, whereas the miR-21 sensor shows some toxicity. This could in fact be due to very low background expression of miR-21 in HEK293 cells[18]. In summary, only the delayed sensor showed selective actuation with this highly potent output.

DISCUSSION

Our study showcases a new strategy to markedly improve the digital behavior of synthetic circuits by judicious recombinase-driven activation of various circuit genes at the appropriate time. In the particular sensor circuit described here, the strategy allows some of the original circuit building blocks to be discarded (i.e., LacI repressor) while still achieving much-improved performance.

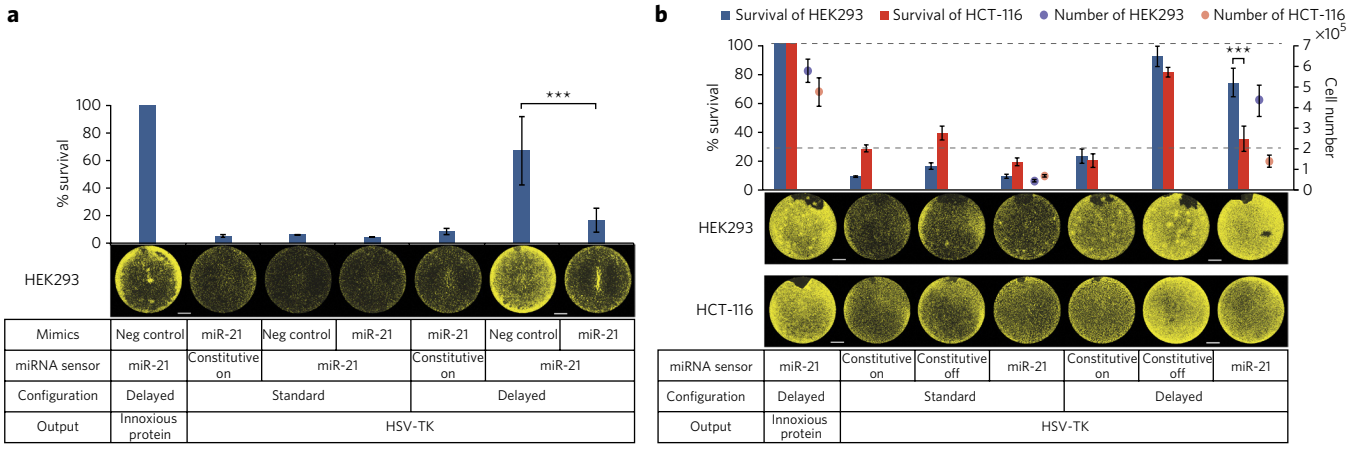

Figure 6 | Selective cytotoxicity in HEK293 and HCT-116 cells with HSV-TK output. The bar charts show cell survival with the indicated circuit and miRNA mimics. Survival is the cell number percentage relative to the control well transfected side by side with nontoxic DsRed-producing sensor (innoxious protein). To illustrate, we show fluorescent images of entire wells stained with a dye for live cells (calcein, AM). Owing to high variability in the absolute staining intensity per cell (as opposed to the number of stained cells), the images cannot be used to make quantitative conclusions. The numbers are measured by flow cytometry and/or cell counting (Online Methods). (**a**) Selective cytotoxicity in HEK293 cells elicited with miR-21 sensor in the presence of miR-21 (on state, cell death expected) or negative (neg) control mimics (off state, cell survival expected). The 'constitutive on' is a double-mutant $LacI^{MUT}$miR-FF4^{MUT} sensor that cannot repress HSV-TK. Individual replicates are shown in **Supplementary Figure 14**. (**b**) Selective cytotoxicity in HEK293 and HCT-116 cells elicited by differential expression of endogenous miR-21 in these cell lines. The constitutive on sensor is a double-mutant $LacI^{MUT}$miR-FF4^{MUT}, and the 'constitutive off' is a sensor with the rtTA and LacI genes furnished with scrambled targets insensitive to miR-21. In addition, absolute numbers of HCT-116 and HEK-293 cells are shown (right axis) for the nontoxic control sensor without HSV-TK output and for miR-21 sensors with HSV-TK output. Individual replicates are in **Supplementary Figure 16**. ***$P < 0.0001$ as calculated using Student's *t*-test. Error bars show ± s.d. using at least three biological replicas. Scale bars, 3 mm.

This greatly facilitates scaling such sensors to larger networks and reduces their DNA payload, opening new venues in biosensing and bioactuation. There is a fixed size cost of a Cre expression cassette; however, the recombinase can be applied simultaneously to multiple miRNA-only switches that are themselves very compact.

Recombinases have been used to control gene expression in genetic engineering applications[40,41] and more recently in biological computing circuits[42] to implement state machines[43], counters[44] and sequential logic[45,46]. Our report highlights one additional dimension of recombinase use in synthetic circuits, namely, their use in controlling the genetic makeup of the circuit in time-dependent fashion. Extension of this approach is likely to open new avenues in synthetic biology research.

Our results demonstrate how temporal control of circuit components could be crucial in conjunction with a highly potent physiological output such as HSV-TK. The leakage in the off state with the standard sensor resulted in toxicity levels similar to those of the on state owing to enzymatic signal amplification, whereas the delayed sensor largely eliminated this undesired outcome. Extremely tight control of individual nodes in a biological network is also conducive to preserving or amplifying the initial input information content. Thus, our approach could enable reliable control of gene expression in small-scale engineered genetic components with potent physiological outputs as well as facilitate digital signal propagation in large synthetic interaction cascades.

Received 17 July 2014; accepted 22 September 2014; published online 14 October 2014

METHODS

Methods and any associated references are available in the online version of the paper.

References

1. Wodarz, A. & Nusse, R. Mechanisms of Wnt signaling in development. *Annu. Rev. Cell Dev. Biol.* **14**, 59–88 (1998).
2. Shimizu, T.S., Tu, Y.H. & Berg, H.C. A modular gradient-sensing network for chemotaxis in *Escherichia coli* revealed by responses to time-varying stimuli. *Mol. Syst. Biol.* **6**, 382 (2010).
3. Mansfield, J.H. *et al.* MicroRNA-responsive 'sensor' transgenes uncover Hox-like and other developmentally regulated patterns of vertebrate microRNA expression. *Nat. Genet.* **36**, 1079–1083 (2004).
4. Zhang, F., Carothers, J.M. & Keasling, J.D. Design of a dynamic sensor-regulator system for production of chemicals and fuels derived from fatty acids. *Nat. Biotechnol.* **30**, 354–359 (2012).
5. Weber, W. *et al.* A synthetic mammalian gene circuit reveals antituberculosis compounds. *Proc. Natl. Acad. Sci. USA* **105**, 9994–9998 (2008).
6. Callura, J.M., Dwyer, D.J., Isaacs, F.J., Cantor, C.R. & Collins, J.J. Tracking, tuning and terminating microbial physiology using synthetic riboregulators. *Proc. Natl. Acad. Sci. USA* **107**, 15898–15903 (2010).
7. Gardner, T.S., Cantor, C.R. & Collins, J.J. Construction of a genetic toggle switch in *Escherichia coli*. *Nature* **403**, 339–342 (2000).
8. Egbert, R.G. & Klavins, E. Fine-tuning gene networks using simple sequence repeats. *Proc. Natl. Acad. Sci. USA* **109**, 16817–16822 (2012).
9. Basu, S., Gerchman, Y., Collins, C.H., Arnold, F.H. & Weiss, R. A synthetic multicellular system for programmed pattern formation. *Nature* **434**, 1130–1134 (2005).
10. de Las Heras, A., Carreno, C.A., Martinez-Garcia, E. & de Lorenzo, V. Engineering input/output nodes in prokaryotic regulatory circuits. *FEMS Microbiol. Rev.* **34**, 842–865 (2010).
11. Liang, J.C., Chang, A.L., Kennedy, A.B. & Smolke, C.D. A high-throughput, quantitative cell-based screen for efficient tailoring of RNA device activity. *Nucleic Acids Res.* **40**, e154 (2012).
12. Weber, W. *et al.* A synthetic time-delay circuit in mammalian cells and mice. *Proc. Natl. Acad. Sci. USA* **104**, 2643–2648 (2007).
13. Elowitz, M.B. & Leibler, S. A synthetic oscillatory network of transcriptional regulators. *Nature* **403**, 335–338 (2000).
14. Prindle, A. *et al.* A sensing array of radically coupled genetic 'biopixels'. *Nature* **481**, 39–44 (2012).
15. Tabor, J.J., Levskaya, A. & Voigt, C.A. Multichromatic control of gene expression in *Escherichia coli*. *J. Mol. Biol.* **405**, 315–324 (2011).
16. Rinaudo, K. *et al.* A universal RNAi-based logic evaluator that operates in mammalian cells. *Nat. Biotechnol.* **25**, 795–801 (2007).
17. Deans, T.L., Cantor, C.R. & Collins, J.J. A tunable genetic switch based on RNAi and repressor proteins for regulating gene expression in mammalian cells. *Cell* **130**, 363–372 (2007).
18. Xie, Z., Wroblewska, L., Prochazka, L., Weiss, R. & Benenson, Y. Multi-input RNAi-based logic circuit for identification of specific cancer cells. *Science* **333**, 1307–1311 (2011).

19. Haynes, K.A., Ceroni, F., Flicker, D., Younger, A. & Silver, P.A. A sensitive switch for visualizing natural gene silencing in single cells. *ACS Synth. Biol.* **1**, 99–106 (2012).
20. Biffi, A. *et al.* Lentiviral hematopoietic stem cell gene therapy benefits metachromatic leukodystrophy. *Science* **341**, 1233158 (2013).
21. Kota, J. *et al.* Therapeutic microRNA delivery suppresses tumorigenesis in a murine liver cancer model. *Cell* **137**, 1005–1017 (2009).
22. Mangan, S. & Alon, U. Structure and function of the feed-forward loop network motif. *Proc. Natl. Acad. Sci. USA* **100**, 11980–11985 (2003).
23. Basu, S., Mehreja, R., Thiberge, S., Chen, M.T. & Weiss, R. Spatiotemporal control of gene expression with pulse-generating networks. *Proc. Natl. Acad. Sci. USA* **101**, 6355–6360 (2004).
24. Sontag, E.D. Remarks on feedforward circuits, adaptation, and pulse memory. *IET Syst. Biol.* **4**, 39–51 (2010).
25. Bleris, L. *et al.* Synthetic incoherent feedforward circuits show adaptation to the amount of their genetic template. *Mol. Syst. Biol.* **7**, 519 (2011).
26. Weber, W., Kramer, B.P. & Fussenegger, M. A genetic time-delay circuitry in mammalian cells. *Biotechnol. Bioeng.* **98**, 894–902 (2007).
27. Dunlop, M.J., Cox, R.S., Levine, J.H., Murray, R.M. & Elowitz, M.B. Regulatory activity revealed by dynamic correlations in gene expression noise. *Nat. Genet.* **40**, 1493–1498 (2008).
28. Hausser, J. *et al.* Timescales and bottlenecks in miRNA-dependent gene regulation. *Mol. Syst. Biol.* **9**, 711 (2013).
29. Hooshangi, S., Thiberge, S. & Weiss, R. Ultrasensitivity and noise propagation in a synthetic transcriptional cascade. *Proc. Natl. Acad. Sci. USA* **102**, 3581–3586 (2005).
30. Schnütgen, F. *et al.* A directional strategy for monitoring Cre-mediated recombination at the cellular level in the mouse. *Nat. Biotechnol.* **21**, 562–565 (2003).
31. Weber, W. *et al.* Macrolide-based transgene control in mammalian cells and mice. *Nat. Biotechnol.* **20**, 901–907 (2002).
32. Matsuda, T. & Cepko, C.L. Controlled expression of transgenes introduced by *in vivo* electroporation. *Proc. Natl. Acad. Sci. USA* **104**, 1027–1032 (2007).
33. Singh, J. & Padgett, R.A. Rates of *in situ* transcription and splicing in large human genes. *Nat. Struct. Mol. Biol.* **16**, 1128–1133 (2009).
34. Leisner, M., Bleris, L., Lohmueller, J., Xie, Z. & Benenson, Y. Rationally designed logic integration of regulatory signals in mammalian cells. *Nat. Nanotechnol.* **5**, 666–670 (2010).
35. Kanegae, Y. *et al.* High-level expression by tissue/cancer-specific promoter with strict specificity using a single-adenoviral vector. *Nucleic Acids Res.* **39**, e7 (2011).
36. Andrade-Rozental, A.F. *et al.* Gap junctions: the "kiss of death" and the "kiss of life". *Brain Res. Brain Res. Rev.* **32**, 308–315 (2000).
37. Mesnil, M., Piccoli, C., Tiraby, G., Willecke, K. & Yamasaki, H. Bystander killing of cancer cells by herpes simplex virus thymidine kinase gene is mediated by connexins. *Proc. Natl. Acad. Sci. USA* **93**, 1831–1835 (1996).
38. Mohr, L. *et al.* Gene therapy of hepatocellular carcinoma *in vitro* and *in vivo* in nude mice by adenoviral transfer of the *Escherichia coli* purine nucleoside phosphorylase gene. *Hepatology* **31**, 606–614 (2000).
39. Mercer, K.E., Ahn, C.E., Coke, A., Compadre, C.M. & Drake, R.R. Mutation of herpesvirus thymidine kinase to generate ganciclovir-specific kinases for use in cancer gene therapies. *Protein Eng.* **15**, 903–911 (2002).
40. Backman, K., Oconnor, M.J., Maruya, A. & Erfle, M. Use of synchronous site-specific recombination *in vivo* to regulate gene-expression. *Bio/Technology* **2**, 1045–1049 (1984).
41. Dale, E.C. & Ow, D.W. Gene-transfer with subsequent removal of the selection gene from the host genome. *Proc. Natl. Acad. Sci. USA* **88**, 10558–10562 (1991).
42. Benenson, Y. Biomolecular computing systems: principles, progress and potential. *Nat. Rev. Genet.* **13**, 455–468 (2012).
43. Ham, T.S., Lee, S.K., Keasling, J.D. & Arkin, A.P. Design and construction of a double inversion recombination switch for heritable sequential genetic memory. *PLoS ONE* **3**, e2815 (2008).
44. Friedland, A.E. *et al.* Synthetic gene networks that count. *Science* **324**, 1199–1202 (2009).
45. Siuti, P., Yazbek, J. & Lu, T.K. Synthetic circuits integrating logic and memory in living cells. *Nat. Biotechnol.* **31**, 448–452 (2013).
46. Bonnet, J., Yin, P., Ortiz, M.E., Subsoontorn, P. & Endy, D. Amplifying genetic logic gates. *Science* **340**, 599–603 (2013).

Acknowledgments

The work was funded the US National Institutes of Health and National Cancer Institute grant 5R01CA155320 and a European Research Council starting grant CellControl. We wish to thank the M. Fussenegger lab in our department for the ET-ETR inducible system, K. Hoelle and L. Prochazka for plasmids and Benenson lab members for discussions. We thank M. Dessing and V. Jaeggin for assistance with flow cytometry and T. Horn for help with imaging. We thank R. Kellogg from S. Tay's laboratory in our department for help with viability assays.

Author contributions

N.L. conceived of the project, designed experiments, performed all the experiments, analyzed data and wrote the paper. Y.B. conceived of and supervised the project, designed experiments, analyzed data and wrote the paper.

Competing financial interests

The authors declare competing financial interests: details accompany the online version of the paper.

Additional information

Supplementary information is available in the online version of the paper. Reprints and permissions information is available online at http://www.nature.com/reprints/index.html Correspondence and requests for materials should be addressed to Y.B.

ONLINE METHODS

Synthetic miRNAs. RNA mimic of human miR-21 and negative control miRNA were purchased from Dharmacon RNAi Technology (Thermo scientific). The miR-21 mimic (cat. No. C-300492-03-0005) is double-stranded RNA that mimics the function of human miRNA-21 (MI0000077). The negative control mimic (cat. no. CN-001000-01-05) is based on a mix of *Caenorhabditis elegans* miRNA sequences. siRNA-FF4 (ref. 16) was purchased from Microsynth AG.

Chemicals. Doxycycline hyclate was purchased from Sigma-Aldrich (Fluka; cat. no. 44577-5G), and a stock solution of 10 mg/ml was prepared in deionized water. Erythromycin was purchased from Sigma-Aldrich (Sigma; cat. no. E5389-1G), and a stock solution of 10 mg/ml was prepared in 100% ethanol. Ganciclovir was purchased from Sigma-Aldrich (Sigma; cat. no. G2536) and stock solution of 2.6 mg/ml (10 mM) was prepared in 2 mM HCl solution in deionized water. Tamoxifen ((Z)-4-Hydroxytamoxifen) was purchased from Sigma-Aldrich (Sigma; cat. no. H7904-5MG) and stock solution of 0.39 mg/ml was prepared in 100% ethanol. Calcein AM was purchased from Life Technologies (cat. no. C3100MP), and tubes with 50 µg were resuspended in 50 µl of 100% DMSO.

Cell culture and transfection. HEK293 (293-H) cell line was purchased from Invitrogen (cat. no. 11631-017). HEK293 cells were cultured in RPMI-1640 medium (GIBCO Life Technologies; cat. no. A10491-01) supplemented with 10% FBS (Sigma), 0.045 g/ml of penicillin and 0.045 g/ml streptomycin at 37 °C, 100% humidity and 5% CO_2. Lipofectamine 2000 transfection reagent (Life Technologies) was used in all experiments. 1.5×10^5 HEK293 cells were seeded in 1 ml RPMI 1640 complete medium into each well of 12-well uncoated plastic plates (Thermo Scientific Nunc) and grown for ~24 h. 2.8 µl of Lipofectamine 2000 were added to each sample, as described in the manual using Optimem (Life Technologies) to resuspend DNA (100 µl/sample) and incubation reagent (100 µl/sample). Medium was changed before transfection with doxycycline to a final dilution of 1 µg/ml. HeLa cell line was purchased from ATCC (cat. no. CCL-2). HeLa cells were cultured in DMEM medium (Life Technologies GIBCO; cat. no.11966-025) supplemented with 10% FBS (Sigma), 4.5 g D-glucose/l, 1 mM nonessential amino acids (Life Technologies GIBCO; cat. no. 11140-035 at 37 °C, 100% humidity and 5% CO_2. HuH-7 cells were purchased from the Health Science Research Resources bank of the Japan Health Sciences Foundation (cat. no. JCRB0403, lot no. 07152011) and cultured at 37 °C, 5% CO2 in DMEM, low glucose, GlutaMAX (Life Technologies, cat. no. 21885-025), supplemented with 10% FBS and 0.045 g/ml of penicillin and 0.045 g/ml streptomycin. HCT-116 were purchased from the Deutsche Sammlung von Mikroorganismen und Zellkulturen (DSMZ) (cat. no. ACC581). HCT-116 cells were grown in the exact same conditions as HeLa (see above). The cell line comparison was performed in 24-well uncoated plastic plates (Thermo Scientific Nunc) following the same protocol as that for the 12-well plate, with plasmid amounts and transfection reagent scaled down by a factor of two. 7.5×10^4 HEK293 cells, 6×10^4 HeLa cells, 4×10^4 HuH-7 cells and 1.5×10^5 HCT-116 cells were seeded in 500 µl of their respective complete medium into each well of 24-well uncoated plastic plates (Thermo Scientific Nunc) and grown for ~24 h. 1.4 µl of Lipofectamine 2000 were added to each sample, as described in the manual using Optimem (Life Technologies) to resuspend DNA (50 µl/sample) and incubation reagent (50 µl/sample). The medium was changed before transfection with doxycycline to a final dilution of 1 µg/ml. Specific plasmid compositions for transfections performed in this manuscript are summarized in **Supplementary Tables 1–15**. Transfected cells were incubated for 3 d before flow cytometry analysis. All reported data are averaged values of three to six biological replicas. The error bars represent ± 1 s.d.

Flow cytometry measurements. All samples were measured ~72 h after transfection (or 5 d for the cell viability assay) with Fortessa flow analyzers (BD Biosciences). DsRed was measured using a 561-nm laser, a 600-nm long pass filter and a 610/20 emission filter with a PMT at 280 V. AmCyan and Cerulean were measured using a 445-nm laser and 473/10 emission filter with a PMT at 280 V. ZsYellow was measured using a 480-nm laser, a 505 long-pass filter and a 542/27 emission filter with a PMT at 220 V. The improvement of the delayed sensor over standard architecture is not sensitive to specific PMT values in the DsRed channel as shown in **Supplementary Figure 17**.

Delayed Cre translocation. Experiments shown in **Figure 3c** were performed as follows: 44 µl of tamoxifen stock solution (0.39 mg/ml) were added to 4 ml of complete RPMI 1640 medium, and 110 µl of the mixture were added into desired wells in the 12-well plate at the time specified. After addition of the drug, the concentration of tamoxifen in the well is 0.39 µg/ml, which is optimal to promote full translocation of the recombinase[32].

Fluorescent microscopy. Fluorescent images were acquired before flow cytometry measurements by an inverted Fluorescent Microscope (Nikon Eclipse Ti) using a Fiber Illuminator (Nikon Intensilight C-HGFI), optimized optical filter sets (Semrock) and a Digital Camera System (Hammamatsu, ORCA R2). Calcein AM was measured with the filter combination YFP HC (HC 500/24, HC 542/27, BS 520) with an exposure time of 300 ms. DsRed was measured with the filter combination TxRed HC (HC 624/40, HC 562/40, BS 593) with an exposure time of 1 s. AmCyan was measured with the filter combination CFP HC (HC 438/24, HC 483/32, BS 458). Microscopy images were contrast-enhanced for better visualization by ImageJ software. For **Figure 4b**, in AmCyan images (16 bits), the intensity of the LUT window was adjusted to 0–12,000; in DsRed images (16 bits), the intensity of LUT window was adjusted to 1,000–5,500. Because the DsRed channel had different backgrounds in HEK293 and HeLa, a background subtraction of 700 units was done in this channel in HeLa cells. In **Figure 5** and **Supplementary Figures 15** and **16**, all images were first converted to 8 bits; in Calcein AM images (8 bits), the intensity of the LUT window was adjusted to 0–60 for HEK293 pictures and 0–50 for HCT-116 pictures.

Time course measurements. Transfections were done in 24-well uncoated plastic plates (Thermo Scientific Nunc), with seeding and transfection reagent scaled down by a factor of two (Cell Culture and Transfection section). 21× DNA master mix for each transfection was prepared, and 1× of each DNA master mix was added to each well individually. Each time course data point comes from a separate transfected well.

Data analysis. Scatter plots and bar charts in all of the main and Supplementary Figures were generated as follows. Gating for DsRed-positive cells (%DsRed$^+$) was determined from AmCyan single color transfection with 99.9% DsRed$^+$ cells outside the gate. Gating for AmCyan-positive cells (%AmCyan$^+$) was determined from DsRed single color transfection with 99.9% AmCyan$^+$ cells outside the gate. Gating examples are shown in **Supplementary Figure 18**. For each sample, we calculated the frequency of DsRed-positive cells (%DsRed$^+$), the mean DsRed value in DsRed-positive cells, mean(DsRed$^+$) and the frequency of AmCyan-positive cells (%AmCyan$^+$). The average signal per transfected cell, denoted as DsRed per cell (AU) "in the main text or" DsRed/Cell, abs. u. in **Supplementary Figures 1, 3, 5, 7, 8, 9, 10, 11, 13** and **15**, was calculated as:

$$\frac{Mean(DsRed^+) \times \%DsRed^+}{\%AmCyan^+}$$

The total signal without normalization, denoted as total DsRed (AU) in the main text or Σ DsRed a.u. in the **Supplementary Figure 2**, was calculated as

$$Mean(DsRed^+) \times \%DsRed^+$$

The frequency of DsRed cells denoted as DsRed$^+$/AmCyan$^+$ in top row in **Supplementary Figure 3**, was calculated as:

$$\frac{\%DsRed^+}{\%AmCyan^+}$$

The relative expression of DsRed signal denoted as DsRed/Cell rel. u. in the middle row in **Supplementary Figure 3**, was calculated as:

$$\frac{Mean(DsRed^+) \times \%DsRed^+}{Mean(AmCyan^+) \times \%AmCyan^+}$$

Error propagation was used to estimate the error of the dynamic ranges and was calculated as:

$$\left\{\sqrt{\left(\frac{SD(Data\,set\,1)}{Mean(Data\,set\,1)}\right)^2 + \left(\frac{SD(Data\,set\,2)}{Mean(Data\,set\,2)}\right)^2}\right\} \times \frac{Mean(Data\,set\,1)}{Mean(Data\,set\,2)},$$

where SD denotes s.d.

Cell viability assay. All of the experiments were performed in 24-well plates. The transfection protocol in HEK293 with miRNA mimics experiments was as described in the Cell Culture and Transfection section. Medium was changed before transfection with doxycycline to a final dilution of 1 µg/ml and ganciclovir to a final concentration of 100 µM. 5 d after transfection, the medium was replaced with a solution of PBS with 1 µM of Calcein AM. Cells were incubated in the dark for 30 min at 37 °C and imaged with a fluorescent microscope. 1 drop/ml of calibration particles (Sphero BD Biosciences; cat. no. 559123) were added to 0.5% Trypsin-EDTA (GIBCO Life Technologies; cat. no. 15400-054). Calcein AM solution was removed, and 200 µl of trypsin with calibration particles was added to each well and incubated for 3 min at 37 °C. Cells were harvested, transferred to FACS tubes (Life Systems Design, cat. no. 02-1412-000) and kept on ice before measurement by flow cytometry. Each tube was sampled for 30 s with Fortessa flow analyzer, and the cell number was inferred as follows. First, cells were gated using forward and side scatter channels, and in this gate, cells positive for Calcein AM were counted. The volume of each sample measured by flow cytometry was normalized using the beads in solutions. The beads were identified with double gating, first selected on FSC and SSC channels, and then gated using Red channel. Finally the number of Calcein^{POS} cells was normalized to the number of beads in this sample to give a measure of cell number in the well. This measure was further normalized against the same measure obtained with the nontoxic control sensor transfected side by side (**Supplementary Fig. 19a**).

The experiments conducted in HEK293 and HCT-116 without mimics use the same transfection protocol as described in the Cell Culture and Transfection section, except that the same number (1×10^5) of HEK293 and HCT-116 cells was seeded 24 h prior to transfection. The cell viability assay was measured as described above. In addition we loaded some samples on an improved counting Neubauer chamber (cat. no. T729.1 Roth AG GMBH) and photographed with a fluorescent microscope. The absolute number of cells per well, was determined from manual counting of Calcein-positive cells in at least 2×1 mm^2 squares from the Neubauer chamber (**Supplementary Fig. 19b**). Cell counting using flow cytometry and Neubauer were extremely well correlated (**Supplementary Fig. 19c**). In **Figure 6**, *P* values were calculated with two-tailed Student's *t*-test.

Plasmid DNA constructs. Standard molecular biology techniques were used. Oligonucleotide sequences used to prepare the plasmid DNA constructs are listed in **Supplementary Table 16**. All plasmids have been sequence verified.

CAGop-Lox2272-LoxP-DsRed$_{Rev}$-Lox2272-LoxP-FF4 (pNL53). DsRed was amplified from CAGop-DsRed-FF5-FF4 (pZ225) with PR1 and PR2. The PCR product replaced eGFP in CAG-Lox2272-LoxP-eGFP$_{Rev}$-Lox2272-LoxP (Addgene no. 28304) using XhoI and KpnI. Lox2272-LoxP-DsRed$_{Rev}$-Lox2272-LoxP was amplified with PR3 and PR4, and the PCR product replaced DsRed-FF5 with Lox2272-LoxP-DsRed$_{Rev}$-Lox2272-LoxP in CAGop-DsRed-FF5-FF4 (pZ225) using NheI and HindII.

CAGop-Lox2272-DsRed-LoxP-FF4 (pNL75). In vitro recombination of 250 ng of CAGop-Lox2272-LoxP-DsRed$_{Rev}$-Lox2272-LoxP-FF4 (pNL53) was done using 1 unit of Cre recombinase (NEB) for 30 min at 37 °C.

TRE-LacI-T21-miR-FF4^{mut}(pNL73). miR-FF4 in TRE-LacI-T21-miR-FF4 (pZ224 in ref. 18) was replaced with the mutant sequence (gBlock1 from IDT) using HindIII and SalI.

TRE-LacI^{mut}-miR-FF4 (pNL74). Insertion of adenosine nucleotide after LacI start codon was done to produce a frameshift mutation. Entire TRE-LacI-T21-miR-FF4 (pZ224 in ref. 18) was amplified with phosphorylated PR5 and PR6, and the PCR product was religated.

TRE- LacI^{mut}-T21-miR-FF4^{mut}(pNL119). TRE-LacI^{mut}-T21-miR-FF4 (pNL74) was digested with NheI and HindIII, and the LacI^{mut}-T21 fragment was inserted in TRE-LacI-T21-miR-FF4^{mut} (pNL73) digested with the same enzymes.

CAGop-Lox2272-LoxP-ZsYellow$_{Rev}$-Lox2272-LoxP-FF4 (pNL98). The construct was assembled from three DNA fragments. CAGop-Lox2272-LoxP-DsRed$_{Rev}$-Lox2272-LoxP-FF4 (pNL53) was digested with XhoI and KpnI. ZsYellow was amplified from the commercial plasmid pZsYellow1-N1 (BD Biosciences Clontech) with PR7 and PR8 and digested with XhoI and AscI. Lox2272-LoxP was amplified from CAGop-Lox2272-LoxP-DsRed$_{Rev}$-Lox2272-LoxP-FF4 (pNL53) with PR9 and PR10 and digested with AscI and KpnI. The three fragments were ligated overnight at 4 °C.

CAGop-Lox2272-ZsYellow-LoxP-FF4 (pNL101). In vitro recombination of 250 ng of CAGop-Lox2272-LoxP- ZsYellow$_{Rev}$-Lox2272-LoxP-FF4 (pNL98) was done using 1 unit of Cre recombinase (NEB) for 30 min at 37 °C.

EF1α–iCre (pEL0154). Described previously[47].

CMV-Lox2272-LoxP-DsRed$_{Rev}$-Lox2272-LoxP-FF4 (pNL84). The CMV promoter from Advanced-tTA commercial plasmid (BD Biosciences Clontech) was digested with SpeI and XbaI. It was used to replace CAGop promoter from CAGop-Lox2272-LoxP-DsRed$_{Rev}$-Lox2272-LoxP-FF4 (pNL53) digested with SpeI and NheI.

CMV-Lox2272-DsRed-LoxP-FF4 (pNL85). The CMV promoter from Advanced-tTA commercial plasmid (BD Biosciences Clontech) was digested with SpeI and XbaI and replaced the CAGop promoter from CAGop-Lox2272-DsRed-LoxP-FF4 (pNL75), which was digested with SpeI and NheI.

CMV-LacI-T21-miR-FF4 (pNL63). LacI-T21-miR-FF4 was removed from TRE-LacI-T21-miR-FF4 (pZ224) with NheI and PciI. The fragment was used to exchange tTA in Advanced-tTA commercial plasmid (BD Biosciences Clontech) using XbaI and PciI.

CMV-LacI^{mut}-T21-miR-FF4 (pNL79). LacI^{mut}-T21-miR-FF4 was digested from TRE-LacI^{mut}-T21-miR-FF4 (pNL74) with NheI and PciI. The fragment was used to replace tTA in Advanced-tTA commercial plasmid (BD Biosciences Clontech) using XbaI and PciI.

CMV-LacI-T21-miR-FF4^{mut}(pNL78). LacI-T21-miR-FF4^{mut} was digested from TRE-LacI-T21-miR-FF4^{mut} (pNL73) with NheI and PciI. The fragment was used to exchange tTA in Advanced-tTA plasmid (BD Biosciences Clontech) using XbaI and PciI.

CMV-FRT-F3-iCre$_{rev}$-FRT-F3 (pNL114). CMV-FRT-F3-Citrine$_{rev}$-miR-145-FRT-F3 (pEL0176) has been described previously[47]. iCre was PCR amplified from EF1α-iCre using PR11 and PR12. The PCR product was used to replace Citrine-miR-145 in CMV-FRT-F3-Citrine$_{rev}$-miR-145-FRT-F3 using HindIII and SbfI.

EF1α-Cerulean (pKH024). Cerulean was PCR amplified with PR13 and PR14 from CMV-Brainbow-2.1 R (Addgene plasmid no. 18723) and inserted in EF1α–eGFP (Addgene plasmid no. 11154) using EcoRI and EagI.

CAG-Cerulean (pNL111). Cerulean was extracted from EF1α-Cerulean with EcoRI and BglII and was used to replace AmCyan in CAG-AmCyan, digested with EcoRI and BamHI.

EF1α–FlpO (pEL0162). Described previously[47].

CMV-ET1 (pEL0190). Described previously[47].

ETR-iCre (pNL23). P_{ETR8}-SEAP (pBP13 (ref. 48)) was provided by the Fussenegger laboratory from our department. iCre was digested with EcoRI and NheI from Addgene plasmid no. 26745 and inserted in P_{ETR8}-SEAP, digested with the same enzymes.

ETR-DsRed (pNL93). P_{ETR8}-SEAP (pBP13 (ref. 48)) was provided by the Fussenegger laboratory from our department. DsRed was digested with NheI and XmaI from CAGop-DsRed-FF4-FF5 (pZ223) and inserted in P_{ETR8}-SEAP between XbaI and AgeI.

CAG-ERT2-iCre-ERT2 (pNL125). Addgene plasmid no. 13777.

SV40-iCre (pNL127). The SV40 promoter was PCR amplified with PR15 and PR16 from sequence synthesized *de novo* by Genescript Inc. (last row of **Supplementary Table 16**) and inserted into EF1α-iCre (pEL0154) using SalI and BamHI to exchange the promoter.

SV40-iCre$_{exon1}$-intron-iCre$_{exon2}$(pNL145). The sequence containing the 5′ exon, the intron and a fragment of the 3′ exon of iCre was synthesized *de novo* (gBlock2 from IDT DNA Inc.), PCR amplified with primer PR17 and PR18 and inserted in SV40-iCre (pNL127) using BamHI and BglII.

SV40-iCre$_{exon1}$-intron-iCre$_{exon2}$-CAGop-Lox2272-LoxP-DsRed$_{Rev}$-Lox2272-LoxP-FF4 (pNL151). PCR amplification of SV40-intron-iCre was done using pNL145 as a template with primers PR19 and PR20. Using Gibson assembly[49], the amplicon was inserted into BsaI-digested CAGop-Lox2272-LoxP-RevDsRed-Lox2272-LoxP (pNL53).

SV40-iCre$_{exon1}$-intron-iCre$_{exon2}$-CAGop-Lox2272-DsRed-LoxP-FF4 (pNL152). PCR amplification of SV40-intron-iCre was done using pNL145 with primers PR19 and PR20. Using Gibson assembly[49], the amplicon was inserted into BsaI-digested CAGop-Lox2272-DsRed-LoxP (pNL75).

CAGop-Lox2272-LoxP-HSV-TK$_{Rev}$-Lox2272-LoxP-FF4 (pNL199). PCR amplification of Herpes simplex virus–thymidine kinase from Addgene

doi:10.1038/nchembio.1680

plasmid no. 21911 (pNL157) was performed using PR21 and PR22 primers. The amplicon replaced Reverse-ZsYellow in CAGop-Lox2272-LoxP-Reverse-ZsYellow-Lox2272-LoxP-FF4 (pNL98) using XhoI and AscI.

CAGop-Lox2272-HSV-TK-LoxP-FF4 (pNL200). PCR amplification of Herpes simplex virus–thymidine kinase from Addgene plasmid no. 21911 (pNL157) was performed using PR21 and PR22 primers. The amplicon replaced ZsYellow in CAGop-Lox2272- ZsYellow -LoxP-FF4 (pNL101) using XhoI and AscI.

CAG-LacI-T21-miR-FF4 (pNL160). LacI-T21-miR-FF4 was digested from TRE-LacI-T21-miR-FF4 (pZ224) using NheI and SalI. The fragment replaced AmCyan in CAG-AmCyan (pZ183) predigested with the same enzymes.

Plasmids reported previously. The following plasmids were reported previously in ref. 18. CAG-AmCyan (pZ183), CAGop-DsRed-FF4-FF5 (pZ223), TRE-LacI-T21-miR-FF4 (pZ224), TRE-LacI-T17-T30a-miR-FF4 (pZ223), TRE-LacI-FF5-miR-FF4 (pZ225), CMV-rtTA-T21 (pZ090), CMV-rtTA-T17-T30a (pZ095), CMV-rtTA-FF5 (pZ091) and pUBI-linker-NOS (pDT7004).

47. Prochazka, L., Angelici, B., Haefliger, B. & Benenson, Y. Highly modular bow-tie gene circuits with programmable dynamic behaviour. *Nat. Commun.* **5**, 4729 (2014).
48. Weber, W., Kramer, B.P., Fux, C., Keller, B. & Fussenegger, M. Novel promoter/transactivator configurations for macrolide- and streptogramin-responsive transgene expression in mammalian cells. *J. Gene Med.* **4**, 676–686 (2002).
49. Gibson, D.G. *et al.* Enzymatic assembly of DNA molecules up to several hundred kilobases. *Nat. Methods* **6**, 343–345 (2009).